THE JOURNAL OF PHYSICAL CHEMISTRY C

Article

pubs.acs.org/JPCC

Tunable Structural, Electronic, and Optical Properties of Layered Two-Dimensional C_2N and MoS_2 van der Waals Heterostructure as Photovoltaic Material

Zhaoyong Guan,[†] Chao-Sheng Lian,[†] Shuanglin Hu,[‡] Shuang Ni,[‡] Jia Li,[§] and Wenhui Duan*[,†,∥]

[†]Department of Physics and State Key Laboratory of Low-Dimensional Quantum Physics and [∥]Collaborative Innovation Center of Quantum Matter, Tsinghua University, Beijing 100084, P. R. China

[‡]Institute of Nuclear Physics and Chemistry, China Academy of Engineering Physics, Mianyang, Sichuan 621900, P. R. China

[§]Key Laboratory of Thermal Management Engineering and Materials, Graduate School at Shenzhen, Tsinghua University, Shenzhen 518055, P. R. China

Supporting Information

ABSTRACT: The nitrogenated porous two-dimensional (2D) material C_2N has been successfully synthesized using a simple wet-chemical reaction, which provides a high-performance way to produce such 2D materials with novel electronic and optical properties. In this work, density functional theory (DFT) calculations were performed to investigate the structural, electronic, and optical properties of the layered C_2N/MoS_2 van der Waals (vdW) heterojunction. The C_2N/MoS_2 heterojunction was found to have a direct band gap of 1.30 eV and to present the typical type-II heterojunction feature, facilitating the effective separation of photogenerated electrons and holes. The calculated band alignment and enhanced optical absorption suggest that the C_2N/MoS_2 heterojunction should exhibit good light-harvesting properties. The vertical strain can effectively tune the electronic properties and optical absorption of the C_2N/MoS_2 heterojunction by changing the interaction between the p_z orbital of C_2N and the d_{z^2} orbital of MoS_2. The moderate band gap, well-separated photogenerated electrons and holes, and enhanced visible-light absorption indicate that the C_2N/MoS_2 heterojunction is a potential photovoltaic structure for solar energy.

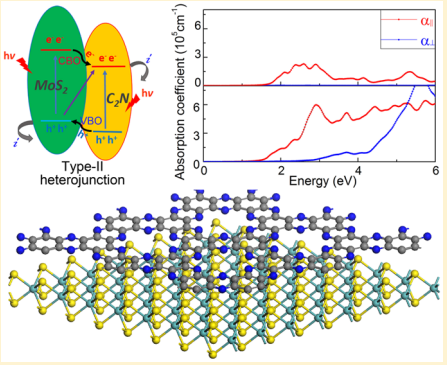

1. INTRODUCTION

Two-dimensional (2D) materials have attracted much attention because of their novel electronic, thermal, and optoelectronic properties.[1−12] In addition to graphene,[1,2] many other 2D systems have also been subjected to extensive studies in recent years, including hexagonal boron nitride (*h*-BN) monolayers,[3−5] transition-metal dichalcogenides (TMDs),[6−10] C_3N_4,[11] and C_2N.[12] MoS_2, as a representative TMD (MX_2),[6−10] has a direct band gap (2.0 eV) and a high carrier mobility in the limit of the single monolayer,[8] making it an important photocatalytic and photovoltaic material.[9,10] Very recently, a C_2N monolayer with uniform pore and nitrogen-atom distributions was synthesized successfully and found to be a semiconductor with a direct band gap of 1.96 eV.[12] The unique electronic properties of C_2N and MoS_2 could be complementary to the use of graphene and *h*-BN in application areas[6−10,12−22] such as catalysis,[13,14] electronics,[15−18] molecular sieves,[19,20] photocatalysis,[12,21,22] and photovoltaics.[8,12] However, a significant challenge still remains for the use of C_2N and MoS_2 in photocatalysis and photovoltaic cells: The charge distributions of their valence-band maximum (VBM) and conduction-band minimum (CBM) states are not well-separated in space, resulting in significantly reduced light-absorbing efficiency because of the fast recombination of photogenerated electrons and holes.[6,12] The construction of heterostructures by stacking different 2D materials on top of each other with interlayer van der Waals (vdW) interactions is a potential way to overcome this weakness.[23,24]

Notably, vdW heterojunctions have the advantage of utilizing the qualities of the stacked 2D materials and have thus been widely investigated;[23−51] examples include graphene/*h*-BN,[34,35] graphene/MoS_2,[38−41] $MX_2/M'X'_2$,[42−51] and C_3N_4/MoS_2 heterojunctions.[23,24] Among the $MX_2/M'X'_2$ vdW heterojunctions, $MoSe_2/MoS_2$,[42,49] WSe_2/MoS_2,[43,44,46,50] $MoSe_2/WSe_2$,[47] and WS_2/MoS_2[48] heterojunctions present type-II band alignments, but their electronic and optical properties are closely related to the stacking order,[51] which does not favor flexible control in experiments.[48] As potential light-harvesting materials, C_2N and MoS_2 monolayers have nearly the same band gaps,[8,12] whereas their work functions differ.[12] Therefore, the C_2N/MoS_2 vdW heterojunction is expected to have a reduced direct band gap that is beneficial for photoabsorption.

Received: December 16, 2016
Revised: January 24, 2017
Published: January 25, 2017

DOI: 10.1021/acs.jpcc.6b12681
J. Phys. Chem. C 2017, 121, 3654−3660

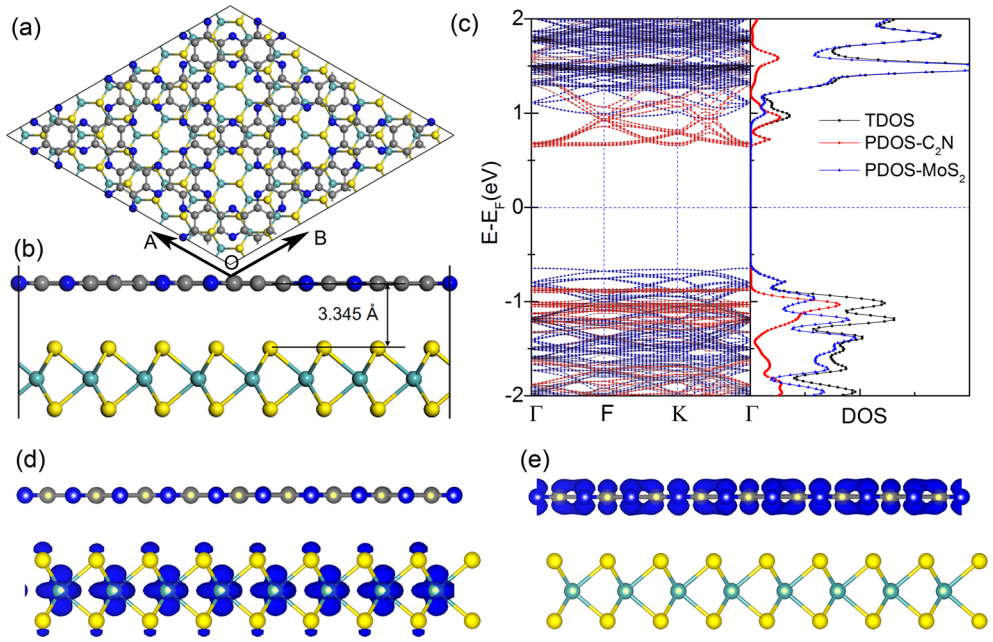

Figure 1. (a,b) Top and side views of the optimized C_2N/MoS_2 heterojunction. (c) Band structure and PDOS of the C_2N/MoS_2 heterojunction. The sizes of the red and blue dots represent the weights of C_2N and MoS_2, respectively. The black, red, and blue lines present the total density of states of the C_2N/MoS_2 heterojunction and the PDOS of C_2N and MoS_2, respectively. The Fermi level (E_F) was set to 0 eV. (d,e) Charge densities of the (d) VBM and (e) CBM of the C_2N/MoS_2 heterojunction. The isovalue was set to 0.03 e Å^{-3}.

It was therefore interesting to investigate whether this heterojunction could show appropriate band alignment to inhibit electron−hole recombination.

In this work, we investigated the C_2N/MoS_2 vdW heterojunction as a potential photovoltaic structure using first-principles calculations. The calculated electronic band structure showed that the C_2N/MoS_2 heterojunction exhibits type-II band-alignment characteristics with a direct band gap of ∼1.3 eV. The type-II band alignment facilitates the separation of photogenerated electrons and holes, as the photogenerated electrons can easily transfer from the MoS_2 layer to the C_2N layer and vice versa for the photogenerated holes. The calculated optical spectra showed enhanced absorption of the visible and ultraviolet light, especially for the in-plane component, implying that the C_2N/MoS_2 vdW heterojunction should exhibit promising photovoltaic properties. The vertical compressive strain was found to effectively tune the band-gap energy and enhance the optical absorption of the C_2N/MoS_2 heterojunction. The C_2N/MoS_2 heterojunction still exhibits the type-II band alignment under certain compressive strains.

2. COMPUTATIONAL DETAILS

Our calculations were performed using density functional theory (DFT) with the projector augmented-wave method,[52] as implemented in the Vienna ab initio simulation package (VASP).[53] The generalized gradient approximation (GGA) was used for the exchange-correlation functional with the Perdew−Burke−Ernzerhof (PBE) parametrization.[54] To accurately describe the vdW interaction, we employed the empirical correction method presented by Grimme (DFT-D2),[55] which has proven to be reliable for describing long-range vdW interactions. As a benchmark, we calculated the distance between bilayer graphene to be 3.25 Å with the PBE + D2 method, with a corresponding binding energy of about 25 meV per carbon atom. These results are in good agreement with previous experimental and theoretical studies.[56,57]

The vacuum region was set to at least 15 Å to avoid virtual interactions between adjacent images. The cutoff energy for plane-wave expansion was 520 eV. For the isolated C_2N and MoS_2 monolayers, the first Brillouin zone integration was performed using Γ-centered 6 × 6 × 1 and 10 × 10 × 1 Monkhorst−Pack k-point samplings, respectively. For the C_2N/MoS_2 heterojunction, we used Γ-centered 2 × 2 × 1 and 3 × 3 × 1 k-point samplings for geometry optimization and electronic structure calculations, respectively. All of the structures were relaxed without any symmetry restriction until the total forces acting on all atoms were less than 0.01 eV/Å.

To investigate the optical absorption properties of the C_2N/MoS_2 heterojunction, we calculated the frequency-dependent dielectric function $[\varepsilon(E)]$ and evaluated the absorption coefficient $[\alpha(E)]$ using the expression[58]

$$\alpha(E) = \frac{4\pi E}{hc}\left[\frac{(\varepsilon_1^{\,2} + \varepsilon_2^{\,2})^{1/2} - \varepsilon_1}{2}\right]^{1/2}$$

where ε_1 and ε_2 represent the real and imaginary parts, respectively, of the frequency-dependent complex dielectric function.[58] Because of the structural anisotropy, anisotropic optical absorption was expected for the heterojunction, with $\alpha(E)^{xx} = \alpha(E)^{yy} \neq \alpha(E)^{zz}$. Correspondingly, the absorption coefficient was divided into two parts: parallel ($\alpha_\parallel$) and perpendicular ($\alpha_\perp$) to the plane of the C_2N monolayer.

3. RESULTS AND DISCUSSION

Before investigating the C_2N/MoS_2 heterojunction, we first explored the structural and electronic properties of isolated C_2N and MoS_2 monolayers. The optimized lattice parameters for the MoS_2 and C_2N monolayers are 3.183 and 8.318 Å, respectively, in good agreement with the experimental measurements and previous theoretical results.[7,12] The C_2N monolayer (Figure S1a) is composed of evenly distributed pores and nitrogen atoms, with C−N distances of 1.336 Å and

DOI: 10.1021/acs.jpcc.6b12681
J. Phys. Chem. C 2017, 121, 3654−3660

C−C distances of 1.427 and 1.467 Å, and all of the atoms are nearly in the same plane. The band structure and partial density of states (PDOS) calculated with the PBE parametrization (see Figure S1b,c) indicate that C_2N is a semiconductor with a direct band gap of 1.66 eV. For the MoS_2 monolayer, we considered only the most stable honeycomb structure (H-MoS_2).[12] The optimized Mo−S distance in the H-MoS_2 monolayer is about 2.413 Å, and the calculated band structure shows that it is a semiconductor with a direct gap of 1.67 eV. These observations are consistent with those of previous reports.[8,12,19,20,59−61]

3.1. Geometric Structure of the C_2N/MoS_2 Heterojunction. In our calculations, the C_2N/MoS_2 heterojunction was constructed based on a supercell model, in which $3 \times 3 \times 1$ C_2N and $8 \times 8 \times 1$ MoS_2 cells were used to match with each other. The supercell used consisted of 354 atoms, including 108 C, 54 N, 64 Mo, and 128 S atoms. The lattice mismatch for this supercell was only 2.3%.

Top and side views of the optimized C_2N/MoS_2 heterojunction are shown in panels a and b, respectively, of Figure 1. In the optimized geometry, the C_2N layer maintains its original planar structure without visible distortion, and MoS_2 also maintains its original plane of hexagonally arranged molybdenum atoms sandwiched between two planes of hexagonally arranged sulfur atoms. The equilibrium distance between the C_2N and MoS_2 layers was calculated to be 3.345 Å, close to the distance (3.280 Å) in a C_2N bilayer with AB stacking.[59] We calculated the binding energy (E_b) of the heterojunction according to the equation

$$E_b = E_{C_2N/MoS_2} - E_{C_2N} - E_{MoS_2}$$

where E_{C_2N/MoS_2}, E_{C_2N}, and E_{MoS_2} are the total energies of the relaxed C_2N/MoS_2 heterojunction, isolated C_2N, and MoS_2 monolayers, respectively. A negative E_b value of −19.98 meV (per atom) was obtained, which indicates that the formation of the C_2N/MoS_2 heterojunction is energetically favorable.

3.2. Electronic Structure and Band Alignment. We next explored the electronic structure of the C_2N/MoS_2 heterojunction. The calculated band structure, shown in Figure 1c, indicates that the C_2N/MoS_2 heterojunction is a semiconductor with a direct band gap of 1.30 eV, which is consistent with the results of PBE-D3 and self-consistent vdW calculations and smaller than those of C_2N (1.66 eV) and MoS_2 (1.67 eV). Hence, electron excitation from the valence band (VB) to the conduction band (CB) would be easier for the C_2N/MoS_2 heterojunction under visible-light irradiation. From the calculated PDOS in Figure 1c, it can be seen that the VBM is mainly provided by the states from the MoS_2 layer whereas the CBM is dominated by the states from the C_2N layer. The valence-band offset (VBO) and conduction-band offset (CBO) between the C_2N and MoS_2 layers were calculated to be about 0.20 and 0.32 eV, respectively. These band-alignment properties suggest that C_2N and MoS_2 form a type-II heterojunction. As illustrated in Figure 2a, the CB and VB of the MoS_2 layer are higher in energy than the corresponding bands of the C_2N layer. When the C_2N/MoS_2 heterojunction is irradiated with light, the electrons can be photoexcited from the valence bands of both the C_2N and MoS_2 sheets. Because of the CBO, the photogenerated electrons in the MoS_2 layer can be transferred to the CB of the C_2N layer. Meanwhile, the VBO promotes the transfer of photogenerated holes from the VB of the C_2N layer to that of the MoS_2 layer. Therefore, both the VBO and CBO promote the redistribution of photogenerated electrons and holes. In addition, the calculated charge densities of the VBM and CBM, shown in Figure 1d,e, indicate that the VBM is made up of the d orbital of MoS_2 whereas the CBM is made up of the p orbital of C_2N, consistent with our detailed PDOS results. The full separation of the charge distributions of the VBM and CBM in the C_2N/MoS_2 heterojunction further promotes the separation of photogenerated electrons and holes, reducing their recombination. More accurate calculations using the Heyd−Scuseria−Ernzerhof (HSE06) hybrid functional (provided in the Supporting Information) confirmed the above results.

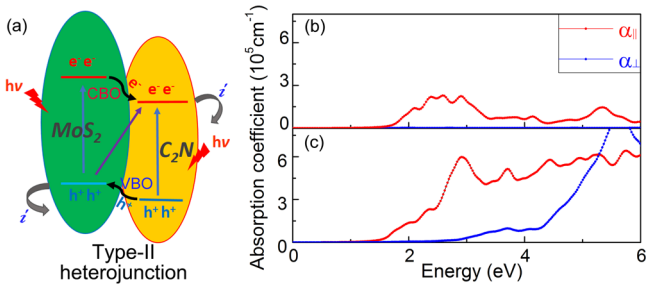

Figure 2. (a) Schematic representation of the band alignment including both VBO and CBO for the C_2N/MoS_2 heterojunction. (b,c) Absorption coefficients of the (b) C_2N monolayer (3×3 supercell) and (c) C_2N/MoS_2 heterojunction. $\alpha_\parallel$ and $\alpha_\perp$ represent the optical absorption coefficients parallel and normal to the plane of the C_2N monolayer, respectively.

3.3. Optical Properties. To investigate the combined effects of C_2N and MoS_2, we calculated the optical properties of both the C_2N monolayer and the C_2N/MoS_2 heterojunction. The obtained optical absorption coefficients with the polarization vector parallel ($\alpha_\parallel$) and normal ($\alpha_\perp$) to the C_2N plane are shown in Figure 2b for the C_2N monolayer. Clearly, the optical absorption is dominated by the $\alpha_\parallel$ component, whereas the contribution of the $\alpha_\perp$ component is negligible. The absorption edge of C_2N is about 1.6 eV, in good agreement with its band gap (1.66 eV). Four absorption peaks were calculated for the $\alpha_\parallel$ component at 2.10, 2.39, 2.59, and 2.90 eV with intensities as large as 2.0×10^5 cm^{-1}, which originate from different interband transitions between the VB and CB of C_2N. These optical behaviors reflect well the ability of the C_2N monolayer to be used in solar cells to absorb visible light (1.61 eV < E < 3.10 eV). The calculated optical absorption coefficients of the C_2N/MoS_2 heterojunction are shown in Figure 2c. The absorption edge is about 1.3 eV, smaller than that of C_2N. The red shift of the absorption edge is due to the fact that, in the C_2N/MoS_2 heterojunction, the photogenerated electrons can be directly excited from the VB of the MoS_2 to the CB of the C_2N. Furthermore, in comparison with the isolated C_2N monolayer, an obvious enhancement of the optical absorption was found for the C_2N/MoS_2 heterojunction. In particular, for the $\alpha_\parallel$ component, four significant absorption peaks appeared at 2.02, 2.33, 2.91, and 3.70 eV with large intensities of 1.38×10^5, 2.28×10^5, 5.97×10^5, and 5.14×10^5 cm^{-1}, respectively. Two absorption peaks at 3.70 and 5.70 eV were also calculated for the $\alpha_\perp$ component with intensities as high as 1.0×10^5 and 8.6×10^5 cm^{-1}, respectively, indicating improved out-of-plane optical absorption compared to that of the isolated C_2N monolayer. In a word, the C_2N/MoS_2 heterojunction was found to exhibit obviously enhanced optical absorption for both visible and ultraviolet light.

DOI: 10.1021/acs.jpcc.6b12681
J. Phys. Chem. C 2017, 121, 3654−3660

3.4. Effect of the Vertical Strain. The vertical strain has proven to be effective in modulating the electronic properties of vdW heterojunctions by changing the interactions between different sheets.[17,62−64] In experiments, one can effectively control the vertical strain applied to the vdW heterojunction by the strain device using diamond anvil cells.[65] Here, we systematically investigated the strain effect in the C_2N/MoS_2 vdW heterojunction. We defined the vertical strain as $\epsilon = d_0 - d$, where d_0 and d are the equilibrium and actual distances, respectively, between the C_2N and MoS_2 sheets. As shown in Figure 3e, with increasing distance between the C_2N and MoS_2 layers, the binding energy was found to rise slowly. For ϵ = −0.2, −0.4, and −0.6 Å, the corresponding E_b values were −19.88, −19.65, and −19.37 meV, respectively. For the compressed strain, the binding energy increased quickly and changed to 0 eV when the distance between the C_2N and MoS_2 sheets approached 2.745 Å (ϵ = 0.6 Å).

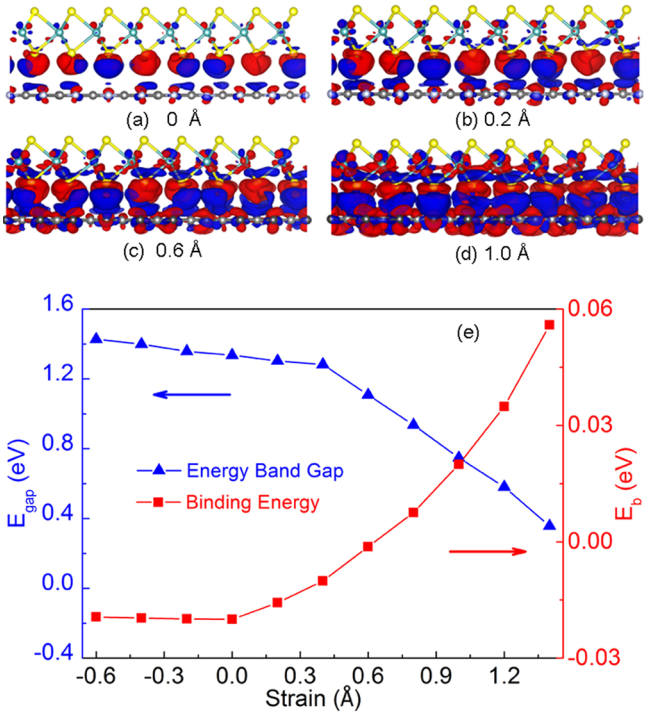

Figure 3. (a−d) Charge density differences of the C_2N/MoS_2 heterojunction with vertical strains: (a) 0, (b) 0.2, (c) 0.6, and (d) 1.0 Å. Blue and red represent charge accumulation and depletion, respectively. (e) Evolution of the band-gap energy E_{gap} and binding energy E_b as a function of the applied strain. The isovalue was set to 0.02 e Å^{-3}.

The change in the interaction between the C_2N and MoS_2 layers should be reflected by the intensity of charge transfer between them. To explore the charge-transfer process, the charge density difference of the C_2N/MoS_2 heterojunction was calculated, as shown in Figure 3a−d for selected strains. For ϵ = 0 Å, a charge redistribution appeared at the interface, and about 0.36 e of charge was determined to be transferred from the MoS_2 layer to the C_2N layer by integrating the differential electron density curve.[66] As the distance between the C_2N and MoS_2 sheets decreased , the charge transfer obviously intensified as a result of the enhanced interlayer interaction. Thus, the electronic behavior of the C_2N/MoS_2 heterojunction is expected to be well tuned by compressive strain.

The calculated band-gap energy (E_{gap}) of the C_2N/MoS_2 heterojunction as a function of the applied strain is shown in Figure 3e, and the evolution of the corresponding PDOS is shown in Figure 4. With increasing compressive strain, the band gap decreased monotonically, as a result of the enhanced interaction between the p_z orbital of C_2N and the d_{z^2} orbital of MoS_2. For ϵ values from −0.6 to 0.3 Å, E_{gap} was found to follow a linear relationship with strain, namely, $E_{gap} = 1.336 - 0.147\epsilon$, whereas for ϵ values in the range 0.4−1.4 Å, a different linear relationship of $E_{gap} = 1.675 - 0.929\epsilon$ was observed. It is noteworthy that, for strains of ϵ < 1.0 Å, the C_2N/MoS_2 heterojunction was always found to present type-II band alignment. As shown in Figure 4f, when the strain increased to 1.2 Å, only C_2N contributed to the CBM whereas both C_2N and MoS_2 contributed to the VBM, thus giving a band alignment that deviated from the type-II band feature. For even larger strains of ϵ > 1.90 Å, the C_2N/MoS_2 heterojunction was found to undergo a semiconductor-to-metal transition, implying tunable conductive and transport properties of this heterojunction.

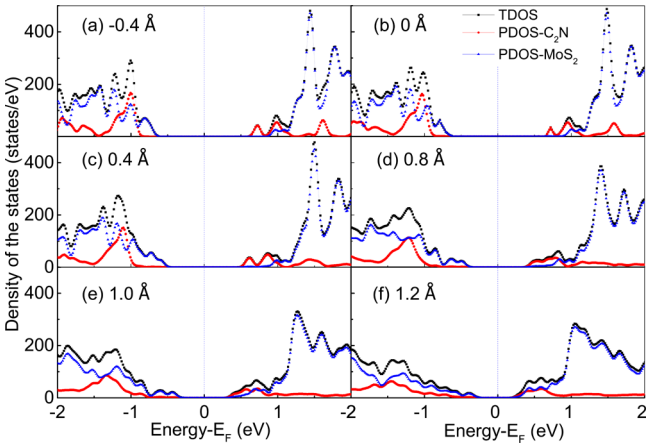

Figure 4. PDOS of the C_2N/MoS_2 heterojunction with vertical strains of (a) −0.4, (b) 0, (c) 0.4, (d) 0.8, (e) 1.0, and (f) 1.2 Å.

Finally, we examined the optical properties of the C_2N/MoS_2 heterojunction under vertical strain. The absorption coefficients calculated for selected strains are shown in Figure 5. With increasing compressive strain, both the $\alpha_{\parallel}$ and $\alpha_{\perp}$ components were found to be significantly red-shifted, consistent with the decrease in the band-gap energy discussed above. There was obvious optical absorption for infrared and visible light. The effective modulation of optical absorption by vertical strain implies wide potential applications of C_2N/MoS_2 heterojunctions in devices for photodetection and photovoltaic structures used in solar cells.

4. SUMMARY

In summary, the structural, electronic, and optical properties of the C_2N/MoS_2 vdW heterojunction were systematically investigated using first-principles calculations. The C_2N/MoS_2 heterojunction presents typical type-II band alignment with a direct band gap of 1.3 eV, which facilitates the effective separation of photogenerated electrons and holes. The calculated band alignment and enhanced optical absorption indicate that the C_2N/MoS_2 vdW heterojunction exhibits good light-harvesting properties. The electronic and optical properties of the C_2N/MoS_2 heterojunction were found to be

DOI: 10.1021/acs.jpcc.6b12681
J. Phys. Chem. C 2017, 121, 3654−3660

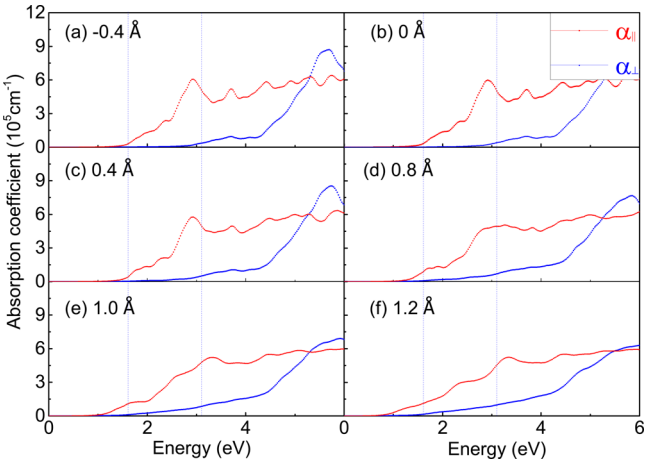

Figure 5. Absorption coefficient of the C_2N/MoS_2 heterojunction with vertical strains (a) −0.4, (b) 0, (c) 0.4, (d) 0.8, (e) 1.0, and (f) 1.2 Å.

effectively tuned by vertical strain through changes in the interaction between the p_z orbital of C_2N and the d_{z^2} orbital of MoS_2. The C_2N/MoS_2 heterojunction with a moderate band gap, well-separated photogenerated electrons and holes, and enhanced visible-light absorption has great potential for use as a photovoltaic heterojunction in solar cells.

■ ASSOCIATED CONTENT

Supporting Information

The Supporting Information is available free of charge on the ACS Publications website at DOI: 10.1021/acs.jpcc.6b12681.

Information on materials, band structure and PDOS of the C_2N monolayer, band structure of the C_2N/MoS_2 heterojunction calculated by PBE-D3, PDOS of the heterojunction calculated by HSE06, and differential electron density curve of the heterojunction (PDF)

■ AUTHOR INFORMATION

Corresponding Author

*E-mail: dwh@phys.tsinghua.edu.cn.

ORCID

Wenhui Duan: 0000-0001-9685-2547

Notes

The authors declare no competing financial interest.

■ ACKNOWLEDGMENTS

We thank Chen Si and Xingxing Li for useful discussions. This work was supported by the Ministry of Science and Technology of China (Grant 2016YFA0301001) and the National Natural Science Foundation of China (Grants 11674188 and 11334006). The computational resources from the SCCAS, Shanghai Supercomputer Center, National Supercomputing Centers of Tianjin and Guangzhou, USTC, and Tsinghua Supercomputer Centers are acknowledged.

■ REFERENCES

(1) Geim, A. K.; Novoselov, K. S. The Rise of Graphene. *Nat. Mater.* **2007**, *6*, 183−191.

(2) Castro Neto, A. H.; Guinea, F.; Peres, N. M. R.; Novoselov, K. S.; Geim, A. K. The Electronic Properties of Graphene. *Rev. Mod. Phys.* **2009**, *81*, 109−162.

(3) Golberg, D.; Bando, Y.; Huang, Y.; Terao, T.; Mitome, M.; Tang, C.; Zhi, C. Boron Nitride Nanotubes and Nanosheets. *ACS Nano* **2010**, *4*, 2979−2993.

(4) Li, J.; Zhou, G.; Chen, Y.; Gu, B.-L.; Duan, W. Magnetism of C Adatoms on BN Nanostructures: Implicationsfor Functional Nanodevices. *J. Am. Chem. Soc.* **2009**, *131*, 1796−1801.

(5) Lin, Y.; Connell, J. W. Advances in 2D Boron Nitride Nanostructures: Nanosheets, Nanoribbons, Nanomeshes, and Hybrids with Graphene. *Nanoscale* **2012**, *4*, 6908−6939.

(6) Ataca, C.; Sahin, H.; Ciraci, S. Stable Single-Layer MX_2 Transition-Metal Oxides and Dichalcogenides in a Honeycomb-Like Structure. *J. Phys. Chem. C* **2012**, *116*, 8983−8999.

(7) Wang, Q. H.; Kalantar Zadeh, K.; Kis, A.; Coleman, J. N.; Strano, M. S. Electronics and Optoelectronics of Two-Dimensional Transition Metal Dichalcogenides. *Nat. Nanotechnol.* **2012**, *7*, 699−712.

(8) Butler, S. Z.; Hollen, S. M.; Cao, L. Y.; Cui, Y.; Gupta, J. A.; Gutiérrez, H. R.; Heinz, T. F.; Hong, S. S.; Huang, J. X.; Ismach, A. F.; et al. Progress, Challenges, and Opportunities in Two-Dimensional Materials Beyond Graphene. *ACS Nano* **2013**, *7*, 2898−2926.

(9) Chhowalla, M.; Shin, H. S.; Eda, G.; Li, L. J.; Loh, K. P.; Zhang, H. The Chemistry of Two-Dimensional Layered Transition Metal Dichalcogenide Nanosheets. *Nat. Chem.* **2013**, *5*, 263−275.

(10) Bonaccorso, F.; Colombo, L.; Yu, G. H.; Stoller, M.; Tozzini, V.; Ferrari, A. C.; Ruoff, R. S.; Pellegrini, V. Graphene, Related Two-Dimensional Crystals, and Hybrid Systems for Energy Conversion and Storage. *Science* **2015**, *347*, 1246501−1246509.

(11) Xiang, Q. J.; Yu, J. G.; Jaroniec, M. Preparation and Enhanced Visible-Light Photocatalytic H_2-Production Activity of Graphene/C_3N_4 Composites. *J. Phys. Chem. C* **2011**, *115*, 7355−7363.

(12) Mahmood, J.; Lee, E. K.; Jung, M.; Shin, D.; Jeon, I.-Y.; Jung, S.-M.; Choi, H.-J.; Seo, J.-M.; Bae, S.-Y.; Sohn, S.-D.; et al. Nitrogenated Holey Two-Dimensional Structures. *Nat. Commun.* **2015**, *6*, 6486−6492.

(13) Ma, D. W.; Wang, Q. G.; Yan, X. W.; Zhang, X. W.; He, C. Z.; Zhou, D. W.; Tang, Y. N.; Lu, Z. S.; Yang, Z. X. 3*d* Transition Metal Embedded C_2N Monolayers as Promising Single-Atom Catalysts: A First-Principles Study. *Carbon* **2016**, *105*, 463−473.

(14) Li, X. Y.; Zhong, W. H.; Cui, P.; Li, J.; Jiang, J. Design of Efficient Catalysts with Double Transition Metal Atoms on C_2N Layer. *J. Phys. Chem. Lett.* **2016**, *7*, 1750−1755.

(15) Kang, J.; Horzum, S.; Peeters, F. M. Heterostructures of Graphene and Nitrogenated Holey Graphene: Moiré Pattern and Dirac Ring. *Phys. Rev. B: Condens. Matter Mater. Phys.* **2015**, *92*, 195419.

(16) Sahin, H. Structural and Phononic Characteristics of Nitrogenated Holy Graphene. *Phys. Rev. B: Condens. Matter Mater. Phys.* **2015**, *92*, 085421.

(17) Wang, D. D.; Han, D. X.; Liu, L.; Niu, L. Structure and Electronic Properties of C_2N/Graphene Predicted by First-Principles Calculations. *RSC Adv.* **2016**, *6*, 28484−28488.

(18) Cao, X.; Shi, J. J.; Zhang, M.; Jiang, X. H.; Zhong, H. X.; Huang, P.; Ding, Y. M.; Wu, M. Band Gap Opening of Graphene by Forming Heterojunctions with the 2D Carbonitrides Nitrogenated Holey Graphene, *g*-C_3N_4, and *g*-CN: Electric Field Effect. *J. Phys. Chem. C* **2016**, *120*, 11299−11305.

(19) Zhu, L.; Xue, Q. Z.; Li, X. F.; Wu, T. T.; Jin, Y. K.; Xing, W. C_2N: an Excellent Two-Dimensional Monolayer Membrane for He Separation. *J. Mater. Chem. A* **2015**, *3*, 21351−21356.

(20) Li, F.; Qu, Y. Y.; Zhao, M. W. Efficient Helium Separation of Graphitic Carbon Nitride Membrane. *Carbon* **2015**, *95*, 51−57.

(21) Mahmood, J.; Jung, S.-M.; Kim, S.-J.; Park, J.; Yoo, J.-W.; Baek, J.-B. Cobalt Oxide Encapsulated in C_2N-h_2D Network Polymer as a Catalyst for Hydrogen Evolution. *Chem. Mater.* **2015**, *27*, 4860−4864.

(22) Lu, X. L.; Xu, K.; Tao, S.; Shao, Z. W.; Peng, X.; Bi, W. T.; Chen, P. Z.; Ding, H.; Chu, W. S.; Wu, C. Z.; et al. Engineering the Electronic Structure of Two-Dimensional Subnanopore Nanosheets Using Molecular Titanium-Oxide Incorporation for Enhanced Photocatalytic Activity. *Chem. Sci.* **2016**, *7*, 1462−1467.

DOI: 10.1021/acs.jpcc.6b12681
J. Phys. Chem. C 2017, 121, 3654−3660

(23) Hou, Y.; Laursen, A. B.; Zhang, J.; Zhang, G.; Zhu, Y.; Wang, X.; Dahl, S.; Chorkendorff, I. Layered Nanojunctions for Hydrogen-Evolution Catalysis. *Angew. Chem., Int. Ed.* **2013**, *52*, 3621−3625.
(24) Wang, J. J.; Guan, Z. Y.; Huang, J.; Li, Q. X.; Yang, J. L. Enhanced Photocatalytic Mechanism for the Hybrid g-C_3N_4/MoS_2 Nanocomposite. *J. Mater. Chem. A* **2014**, *2*, 7960−7966.
(25) Geim, A. K.; Grigorieva, I. V. Van der Waals Heterostructures. *Nature* **2013**, *499*, 419−425.
(26) Furchi, M. M.; Pospischil, A.; Libisch, F.; Burgdorfer, J.; Mueller, T. Photovoltaic Effect in an Electrically Tunable van der Waals Heterojunction. *Nano Lett.* **2014**, *14*, 4785−4791.
(27) Withers, F.; Del Pozo-Zamudio, O.; Mishchenko, A.; Rooney, A. P.; Gholinia, A.; Watanabe, K.; Taniguchi, T.; Haigh, S. J.; Geim, A. K.; Tartakovskii, A. I.; et al. Light-Emitting Diodes by Band-Structure Engineering in van der Waals Heterostructures. *Nat. Mater.* **2015**, *14*, 301−306.
(28) Rivera, P.; Seyler, K. L.; Yu, H.; Schaibley, J. R.; Yan, J.; Mandrus, D. G.; Yao, W.; Xu, X. Valley-Polarized Exciton Dynamics in a 2*d* Semiconductor Heterostructure. *Science* **2016**, *351*, 688−691.
(29) Zhu, X.; Monahan, N. R.; Gong, Z.; Zhu, H.; Williams, K. W.; Nelson, C. A. Charge Transfer Excitons at van der Waals Interfaces. *J. Am. Chem. Soc.* **2015**, *137*, 8313−8320.
(30) Zhou, S. Y.; Gweon, G. H.; Fedorov, A. V.; First, P. N.; de Heer, W. A.; Lee, D. H.; Guinea, F.; Castro Neto, A. H.; Lanzara, A. Substrate-Induced Bandgap Opening in Epitaxial Graphene. *Nat. Mater.* **2007**, *6*, 770−775.
(31) Li, X.; Chen, W.; Zhang, S.; Wu, Z.; Wang, P.; Xu, Z.; Chen, H.; Yin, W.; Zhong, H.; Lin, S. 18.5% Efficient Graphene/GaAs van der Waals Heterostructure Solar Cell. *Nano Energy* **2015**, *16*, 310−319.
(32) Xia, C.; Xue, B.; Wang, T.; Peng, Y.; Jia, Y. Interlayer Coupling Effects on Schottky Barrier in the Arsenene-Graphene van der Waals Heterostructures. *Appl. Phys. Lett.* **2015**, *107*, 193107−193111.
(33) Li, Y.; Xu, C. Y.; Qin, J. K.; Feng, W.; Wang, J. Y.; Zhang, S.; Ma, L. P.; Cao, J.; Hu, P. A.; Ren, W.; et al. Tuning the Excitonic States in MoS_2/Graphene van der Waals Heterostructures via Electrochemical Gating. *Adv. Funct. Mater.* **2016**, *26*, 293−302.
(34) Hunt, B.; Sanchez-Yamagishi, J. D.; Young, A. F.; Yankowitz, M.; Le-Roy, B. J.; Watanabe, K.; Taniguchi, T.; Moon, P.; Koshino, M.; Jarillo-Herrero, P.; et al. Massive Dirac Fermions and Hofstadter Butterfly in a van der Waals Heterostructure. *Science* **2013**, *340*, 1427−1430.
(35) Jung, J.; DaSilva, A. M.; MacDonald, A. H.; Adam, S. Origin of Band Gaps in Graphene on Hexagonal Boron Nitride. *Nat. Commun.* **2015**, *6*, 6308−6318.
(36) Deng, Y.; Luo, Z.; Conrad, N. J.; Liu, H.; Gong, Y.; Najmaei, S.; Ajayan, P. M.; Lou, J.; Xu, X.; Ye, P. D. Black Phosphorus-Monolayer MoS_2 van der Waals Heterojunction *p-n* Diode. *ACS Nano* **2014**, *8*, 8292−8299.
(37) Padilha, J. E.; Fazzio, A.; da Silva, A. J. R. Van der Waals Heterostructure of Phosphorene and Graphene: Tuning the Schottky Barrier and Doping by Electrostatic Gating. *Phys. Rev. Lett.* **2015**, *114*, 066803.
(38) Hou, Y.; Laursen, A. B.; Zhang, J.; Zhang, G.; Zhu, Y.; Wang, X.; Dahl, S.; Chorkendorff, I. Layered Nanojunctions for Hydrogen-Evolution Catalysis. *Angew. Chem., Int. Ed.* **2013**, *52*, 3621−3625.
(39) Roy, K.; Padmanabhan, M.; Goswami, S.; Sai, T. P.; Ramalingam, G.; Raghavan, S.; Ghosh, A. Graphene−MoS_2 Hybrid Structures for Multifunctional Photoresponsive Memory Devices. *Nat. Nanotechnol.* **2013**, *8*, 826−830.
(40) Yu, L.; Lee, Y. H.; Ling, X.; Santos, E. J. G.; Shin, Y. C.; Lin, Y.; Dubey, M.; Kaxiras, E.; Kong, J.; Wang, H.; et al. Graphene/MoS_2 Hybrid Technology for Large-Scale Two-Dimensional Electronics. *Nano Lett.* **2014**, *14*, 3055−3063.
(41) Lu, C.-P.; Li, G.; Watanabe, K.; Taniguchi, T.; Andrei, E. Y. MoS_2: Choice Substrate for Accessing and Tuning the Electronic Properties of Graphene. *Phys. Rev. Lett.* **2014**, *113*, 156804.
(42) Ceballos, F.; Bellus, M. Z.; Chiu, H. Y.; Zhao, H. Ultrafast Charge Separation and Indirect Exciton Formation in a MoS_2-$MoSe_2$ van der Waals Heterostructure. *ACS Nano* **2014**, *8*, 12717−12724.
(43) Cheng, R.; Li, D.; Zhou, H.; Wang, C.; Yin, A.; Jiang, S.; Liu, Y.; Chen, Y.; Huang, Y.; Duan, X. Electroluminescence and Photocurrent Generation from Atomically Sharp WSe_2/MoS_2 Heterojunction *p-n* Diodes. *Nano Lett.* **2014**, *14*, 5590−5597.
(44) Chiu, M. H.; Li, M. Y.; Zhang, W.; Hsu, W. T.; Chang, W. H.; Terrones, M.; Terrones, H.; Li, L. J. Spectroscopic Signatures for Interlayer Coupling in MoS_2-WSe_2 van der Waals Stacking. *ACS Nano* **2014**, *8*, 9649−9656.
(45) Shim, G. W.; Yoo, K.; Seo, S. B.; Shin, J.; Jung, D. Y.; Kang, I. S.; Ahn, C. W.; Cho, B. J.; Choi, S. Y. Large-Area Single-Layer $MoSe_2$ and Its van der Waals Heterostructures. *ACS Nano* **2014**, *8*, 6655−6662.
(46) Jeon, P. J.; Min, S. W.; Kim, J. S.; Raza, S. R. A.; Choi, K.; Lee, H. S.; Lee, Y. T.; Hwang, D. K.; Choi, H. J.; Im, S. Enhanced Device Performances of WSe_2-MoS_2 van der Waals Junction p-n Diode by Fluoropolymer Encapsulation. *J. Mater. Chem. C* **2015**, *3*, 2751−2758.
(47) Rivera, P.; Schaibley, J. R.; Jones, A. M.; Ross, J. S.; Wu, S.; Aivazian, G.; Klement, P.; Seyler, K.; Clark, G.; Ghimire, N. J.; et al. Observation of Long-Lived Interlayer Excitons in Monolayer $MoSe_2$-WSe_2 Heterostructures. *Nat. Commun.* **2015**, *6*, 6242−6247.
(48) Yu, Y.; Hu, S.; Su, L.; Huang, L.; Liu, Y.; Jin, Z.; Purezky, A. A.; Geohegan, D. B.; Kim, K. W.; Zhang, Y.; et al. Equally Efficient Inter Layer Exciton Relaxation and Improved Absorption in Epitaxial and Nonepitaxial MoS_2/WS_2 Heterostructures. *Nano Lett.* **2015**, *15*, 486−491.
(49) Long, R.; Prezhdo, O. V. Quantum Coherence Facilitates Efficient Charge Separation at a MoS_2/$MoSe_2$ van der Waals Junction. *Nano Lett.* **2016**, *16*, 1996−2003.
(50) Nourbakhsh, A.; Zubair, A.; Dresselhaus, M. S.; Palacios, T. Transport Properties of a MoS_2/WSe_2 Heterojunction Transistor and Its Potential for Application. *Nano Lett.* **2016**, *16*, 1359−1366.
(51) He, J. G.; Hummer, K.; Franchini, C. Stacking Effects on the Electronic and Optical Properties of Bilayer Transition Metal Dichalcogenides MoS_2, $MoSe_2$, WS_2, and WSe_2. *Phys. Rev. B: Condens. Matter Mater. Phys.* **2014**, *89*, 075409.
(52) Blöchl, P. E. Projector Augmented-Wave Method. *Phys. Rev. B: Condens. Matter Mater. Phys.* **1994**, *50*, 17953−17979.
(53) Kresse, G.; Furthmüller, J. Efficient Iterative Schemes for Ab Initio Total-Energy Calculations Using a Plane-Wave Basis Set. *Phys. Rev. B: Condens. Matter Mater. Phys.* **1996**, *54*, 11169−11186.
(54) Perdew, J. P.; Burke, K.; Ernzerhof, M. Generalized Gradient Approximation Made Simple. *Phys. Rev. Lett.* **1996**, *77*, 3865−3868.
(55) Bučko, T.; Hafner, J.; Lebègue, S.; Ángyán, J. G. Improved Description of the Structure of Molecular and Layered Crystals: Ab Initio DFT Calculations with van der Waals Corrections. *J. Phys. Chem. A* **2010**, *114*, 11814−11824.
(56) Baskin, Y.; Meyer, L. Lattice Constants of Graphite at Low Temperatures. *Phys. Rev.* **1955**, *100*, 544−544.
(57) Zacharia, R.; Ulbricht, H.; Hertel, T. Interlayer Cohesive Energy of Graphite from Thermal Desorption of Polyaromatic Hydrocarbons. *Phys. Rev. B: Condens. Matter Mater. Phys.* **2004**, *69*, 155406.
(58) Li, X. X.; Zhao, J.; Yang, J. L. Semihydrogenated BN Sheet: A Promising Visible-Light Driven Photocatalyst for Water Splitting. *Sci. Rep.* **2013**, *3*, 1858.
(59) Zhang, R. Q.; Li, B.; Yang, J. L. Effects of Stacking Order, Layer Number and External Electric Field on Electronic Structures of Few-Layer C_2N-h_2D. *Nanoscale* **2015**, *7*, 14062−14070.
(60) Sahin, H. Structural and Phononic Characteristics of Nitrogenated Holey Graphene. *Phys. Rev. B: Condens. Matter Mater. Phys.* **2015**, *92*, 085421.
(61) Du, J.; Xia, C. X.; Xiong, W. Q.; Zhao, Xu.; Wang, T. X.; Jia, J. Tuning the Electronic Structures and Magnetism of Two-Dimensional Porous C_2N via Transition Metal Embedding. *Phys. Chem. Chem. Phys.* **2016**, *18*, 22678−22686.
(62) Huang, L.; Li, Y.; Wei, Z.; Li, J. Strain Induced Piezoelectric Effect in Black Phosphorus and MoS_2 van der Waals Heterostructure. *Sci. Rep.* **2015**, *5*, 16448−16454.
(63) Liu, X. G.; Li, Z. Y. Electric Field and Strain Effect on Graphene−MoS_2 Hybrid Structure: Ab Initio Calculations. *J. Phys. Chem. Lett.* **2015**, *6*, 3269−3275.

DOI: 10.1021/acs.jpcc.6b12681
J. Phys. Chem. C 2017, 121, 3654−3660

(64) Si, C.; Lin, Z. Z.; Zhou, J.; Sun, Z. M. Controllable Schottky Barrier in GaSe/Graphene Heterostructure: the Role of Interface Dipole. *2D Mater.* **2017**, *4*, 015027.
(65) Yankowitz, M.; Watanabe, K.; Taniguchi, T.; San-Jose, P.; LeRoy, B. J. Pressure-Induced Commensurate Stacking of Graphene on Boron Nitride. *Nat. Commun.* **2016**, *7*, 13168−13175.
(66) He, W.; Li, Z. Y.; Yang, J. L.; Hou, J. G. Electronic Structures of Organic Molecule Encapsulated BN Nanotube under Transverse Electric Field. *J. Chem. Phys.* **2008**, *129*, 024710.

DOI: 10.1021/acs.jpcc.6b12681
J. Phys. Chem. C 2017, 121, 3654−3660